Growth of cement hydration products on single walled carbon nanotubes

Makar, J. M.; Chan, G. W.

Publisher's version / Version de l'éditeur:
https://doi.org/10.1111/j.1551-2916.2009.03055.x
Journal of the American Ceramic Society, 92, 6, pp. 1303-1310, 2009-10-01

Growth of cement hydration products on single walled carbon nanotubes

NRCC-50817

Makar, J.M.; Chan, G.W.

October 2009

A version of this document is published in / Une version de ce document se trouve dans:
Journal of the American Ceramic Society, 92, (6), pp. 1303-1310, DOI: 10.1111/j.1551-2916.2009.03055.x

Growth of Cement Hydration Products on Single Walled Carbon Nanotubes

J.M. Makar* and G.W. Chan
Institute for Research in Construction
National Research Council Canada
K1A 0R6

Abstract

Single walled carbon nanotubes (SWCNT) were distributed on the surface of ordinary Portland cement (OPC) grains. The OPC/SWCNT composite was then hydrated at a 0.5 w/c ratio. The effects of the SWCNT on the early hydration process were studied using isothermal conduction calorimetry, high resolution scanning electron microscopy and thermogravimetric analysis. The observed behaviour of the composite samples was compared to both OPC sonicated without SWCNT and previously published data on as-delivered OPC. The SWCNT were found to accelerate the hydration reaction of the C_3S in the OPC. The morphology of both the initial C_3A and the C_3S hydration products were found to be affected by the presence of the SWCNT. In particular, the nanotubes appeared to act as nucleating sites for the hydration products, with the nanotubes becoming rapidly coated with C-S-H. The resulting structures remained on the surface of the cement grains while those in the sonicated and as-delivered OPC samples grew out from the grain surfaces to form typical C-S-H clusters. Classical evidence of reinforcing behaviour, in the form of fiber pullout of the SWCNT bundles, was observed by 24 hours of hydration.

*corresponding author: jon.makar@nrc-cnrc.gc.ca

Introduction

Carbon nanotubes have garnered great interest for their potential as reinforcements in composite materials. Their unique physical properties, including ultra high strength[1], modulus of elasticity[2], elastic behaviour[3] and aspect ratios[4] all suggest that they should be close to ideal reinforcing materials. These properties have led to considerable effort towards their development. Most work to date has focused on polymer composites[5], with other matrix materials such as metals also drawing interest[6]. There has also been significant interest in producing carbon nanotube composites with ceramic matrices[7-10], but less attention has been paid to cements as a potential matrix material. Cements are reactive ceramics that undergo hydration reactions upon exposure to water. As such, they have complex physical structures composed of a variety of hydration reaction products, with their structure changing and developing as the hydration reaction progresses. The most common and industrially important form of cement is ordinary Portland cement (OPC), which forms the binder in concrete after hydration. OPC is primarily composed of tricalcium silicate ($3CaO \bullet SiO_2$ or C_3S in cement chemistry notation), in addition to dicalcium silicate ($3CaO \bullet SiO_2$ or C_2S), tricalcium aluminate ($3CaO \bullet Al_2O_3$ or C_3A), and tetracalcium aluminoferrite ($4CaO \bullet Al_2O_3 \bullet Fe_2O_3$ or C_4AF). Gypsum or other forms of calcium sulphate are added to the Portland cement during manufacture to control the rapid reaction of C_3A at the beginning of the OPC hydration process. The C_3S and C_2S in OPC react with water to form calcium silicate hydrates (C-S-H) and calcium hydroxide, while a variety of hydration products may be formed from the C_3A and C_4AF reactions[11].

Most work to date on cement/carbon nanotube composites has been performed using multi-walled carbon nanotubes (MWCNT) in an OPC matrix. A number of workers have reported on the mechanical properties these composites[12-16], while others have examined their electrical properties[17,18]. The results of the mechanical testing have been inconsistent, with some

reports showing significant improvement in properties and others noticeable deterioration as compared to pure OPC samples.

In contrast, the work reported here focuses on OPC composite materials made with single walled carbon nanotubes (SWCNT). SWCNT have significant advantages over MWCNT for this purpose in terms of higher aspect ratios and diameters of individual tubes that are close to estimates of the structural spacing of C-S-H layers[19]. Past work[20] has shown that the addition of SWCNT to OPC can result in improvements of Vicker's hardness (a correlate to compressive strength[21]) of up to six times the values measured in pure OPC samples hydrated for the same time at the same ratio of water to cement (w/c). However, this difference occurred during the early stages of hydration and largely disappeared after 14 days, a result that suggested that the SWCNT were affecting the hydration behaviour of the OPC, rather than simply acting as a reinforcement. Here we examine the effect of 1% SWCNT content on the early stages of hydration in OPC using isothermal conduction calorimetry, high resolution scanning electron microscopy (SEM) and thermogravimetric analysis (TGA). The behaviour observed for samples with SWCNT is compared to control samples without SWCNT otherwise subjected to the same processing techniques, as well as to recently published work on as-delivered OPC[22].

Experimental Details

Samples were prepared from Canadian GU (U.S. Type 1 equivalent) OPC (Lafarge Canada) and from high quality single walled carbon nanotubes supplied by the National Research Council Canada's Steacie Institute of Molecular Studies. The SWCNT were produced by laser ablation[23] and purified using a solvent based method that does not functionalize the nanotubes[24]. SEM examination of the SWCNT purified by this method shows clean nanotube bundles and some carbon nanoparticles, with purities of about 99%. Details of the OPC manufactured at the Lafarge plant have been presented elsewhere[22]. Samples of the OPC were sonicated for 2 hours

in isopropanol both with and without a 1% by mass content of SWCNT. The isopropanol was then removed in each case by dessication in a vacuum system and the processed samples were stored under vacuum until needed.

Two gram samples of each sonicated material and a five gram sample of the as-delivered OPC were hydrated in polyethylene containers in a Thermometric Tam Air Isothermal Calorimeter (model 3114) using Accusolv (Anachemia, Inc.) water with a maximum impurity level of 1 ppm at a w/c ratio of 0.5 by mass at 23.0^{o} C. Measurements were made at 1 minute time intervals, with data recorded with an uncertainty of ±0.002 mW/g and results reported on a per gram of cement basis. Although only the results from a single type of cement are presented here, the same effects were observed in samples produced with OPC from two additional sources. The results of the conduction calorimetry measurements were then examined and specific hydration durations were chosen for subsequent SEM examination. Times of 0, 60, 120, 135, 180 and 240 minutes were chosen for the samples sonicated with SWCNT and times of 0, 60, 135, 150, 180 and 240 minutes were chosen for the samples sonicated without SWCNT. These times were chosen to correspond to the end of the initial C_3A hydration, the induction period and the initiation of main C_3S hydration reaction. The samples were flash frozen in glass tubes in liquid nitrogen and then freeze dried using a vacuum system at liquid nitrogen temperatures in order to maintain their morphology for SEM examination. This method has been shown to best preserve sample morphology during drying[25,26]. Fourteen to sixteen different grains were then imaged for each sample time at 1.2 kV accelerating voltages, 2.8 mm working distance and 7 μA using a FEG-SEM. Further details of the sample preparation methods, the use of the FEG-SEM for imaging hydrating OPC at this time period and the imaging conditions can also be found elsewhere[22].

In addition to qualitative analysis of the morphologies of hydration products, image analysis was conducted to determine the average surface area covered by C_3A hydration products formed during the first sixty minutes of hydration. The boundaries of each individual structure in each image were highlighted and then the total surface area for that image was calculated using RML-Image software (RML-Image, Varennes, Quebec, Canada). The average values for the images from each type of sample were then determined.

The total heat of hydration was calculated by integration of the heat flow data from the isothermal conduction calorimeter. Additional samples were then prepared as above in order to investigate the effect of the SWCNT on the relative proportion of calcium hydroxide to C-S-H produced during the hydration reaction. Hydration of these samples was stopped by evacuation at five different times (4, 6, 8, 16 and 24 hours for the composite material and 4, 6.6, 9, 20, and 31 hours for the sonicated control sample) so that the total heat produced by the reactions was the same for each pair of times. Thermogravimetric analysis (TGA) was conducted using a heating rate of 10^{o} C/minute on each of these samples to determine the total amount of calcium hydroxide present. Hydrated material was also freeze-dried for SEM examination after 8 and 24 hours hydration for the cement/SWCNT composite and 9 and 31 hours for the sonicated OPC. The latter samples were then broken apart in a mortar and pestle to expose fracture surfaces for imaging, which used the same working conditions as the earlier samples.

Finally, pore water was extracted from the as-delivered and sonicated cement pastes at hydration times of 60, 90, 120, 150, and 240 minutes by placing them in a funnel on fine porosity, slow flow rate filter paper and vacuum filtering. The pore water was collected in 15 ml polystyrene conical test tubes placed in liquid nitrogen as a cold trap. Once the solutions had thawed, they were diluted to 100ml in volumetric flasks. Calcium ion concentration was determined using a Brinkmann Metrohm 808 Titrando automatic titrator with a calcium ion

selective electrode and a Brinkmann double junction silver chloride / potassium chloride reference electrodes after calibration with a series of diluted calcium standard solutions. This measurement was not performed on the SWCNT samples in order to avoid the risk of SWCNT of the measurement equipment.

Results

Figure 1a shows the isothermal conduction calorimetry results for each material under investigation. The numbers in the figure identify the peaks as: 1) initial C_3A reactions; 2) C_3S surface reactions at the end of the induction period[22]; 3) the main C_3S hydration peak; and 4) ettringite formation. In comparison with the as-delivered material, sonication of the OPC accelerated the end of the induction period (Figure 1b), but reduced the maximum heat flow from the cement. The SWCNT composite sample showed a further reduction in the time of the end of the induction period beyond that seen for the sonicated OPC without nanotubes. The heat of hydration for each of the materials as calculated by integrating the heat flow data is shown in Figure 1c. The dots in the figure show the times of samples taken for TGA. The sonicated OPC has a significantly lower heat of hydration as compared to the as-delivered and composite samples after the initial 6 hours of hydration , while the OPC with SWCNT sample initially has the highest heat of hydration, but falls somewhat below that of the as-delivered sample after the first day.

Figure 1b shows the individual data points recorded by the isothermal conduction calorimeter and the details of the behaviour of peak 2 at the end of the induction period. Peak 2 has recently been found to be associated with the formation of pores in the surface of the cement grain and the initial formation of C-S-H on the surface of the cement grains. Increasing amounts C_3A hydration products on the surface of the OPC grain were found to reduce the extent of the peak[22]. The results of Figure 1b therefore suggest that the highest level of initial surface activity

was found in the composite sample, with the lowest level in the sample with sonicated OPC. Figure 1d shows the corresponding heat flow from the very early hydration period, where C_3A was reacting with calcium sulphate to form early hydration products, and in particular, ettringite. There was a similar level of heat flow and hence degree of reaction for the two sonicated samples. In both cases the maximum heat flow was approximately 50% higher than that produced by the as-delivered OPC, although the high levels of heat flow were maintained for a longer time for the sample with SWCNT.

As with other forms of derivative analysis such as derivative thermogravimetric analysis, examination of the derivative of the heat flow (Figure 1e) has been found to give additional information on the properties under investigation[27,28]. In the case of conduction calorimetry, the analysis of the heat flow derivative clarifies the timing of events in the hydration process and allows for a greater level of numerical analysis of those events. In particular, Figure 1a showed that the time for the maximum heat flow in the sample of OPC sonicated with SWCNT was accelerated compared to the control sample. The derivative analysis also shows that timing of the initial reaction at the end of the induction period (inset in Figure 1e) was accelerated by sonication of the OPC and further accelerated by the presence of the SWCNT. The maximum value of the derivative heat flow in the main part of the figure at peak 3 was also significantly increased by the presence of the SWCNT. However, the timing of that maximum, although earlier than that of the unsonicated sample, was the same for both types of sonicated samples, , whether or not the SWCNT were present. The presence of the SWCNT altered the magnitude of the curve at this point, but not its timing. Figure 1e also shows that there was little difference in the peak 4 behaviour, attributed to C_3A hydration reactions[29], between the as-delivered OPC and that sonicated with SWCNT. In comparison, the comparable reaction for the sonicated OPC is spread out in time and does not have a well defined peak It is, however, clear that the reaction is

still taking place, as a pure C_3S reaction would be expected to produce a negative peak in the region between 7 and 15 hours, rather than the flattened curve seen in the figure after the point of maximum heat flow (0 derivative) from the C_3S reaction[27].

Measurements of concentration of calcium ions in the pore water of the as-delivered and sonicate OPCs are shown in Table 1. They appear to follow the general trend reported in the literature for C_3S[30,31] of an initial plateau in concentration, followed by an increase to a maximum value and a subsequent decrease to a concentration closer to the equilibrium value expected for calcium hydroxide. However, the sonicated OPC has lower ion concentrations for the first two hours of hydration than the as-delivered OPC, and larger concentrations thereafter. The maximum concentration of Ca^{2+} for the sonicated OPC was substantially higher than that reported in the literature, while the final value for the as-delivered OPC was less than would typically be expected[30,31].

SEM imaging of the sonicated OPC with SWCNT before hydration showed that the SWCNT appeared to be well distributed in fine bundles across the cement grains. Almost all bundles were less than 20 nm across and the nanotubes were in general finely enough distributed across the surface that they were difficult to discern against the background material. In some cases the images showed fine (5nm-10nm across) networks on the cement grain surface (Figure 2), while in others only traces of nanotube bundles of similar size were identified. Although the fine networks were not easily identified on all grains, the consistent development of hydration products described below suggests that the SWCNT were indeed finely distributed across the cement grains. Similar features were not observed on the surface of the OPC sonicated without SWCNT.

Both types of sonicated samples had a higher number of fine particles distributed across the OPC surface than were observed for as-delivered samples[22]. The accelerated C_3A reactions

shown in Figure 1d suggest that these particles may have been composed of C_3A or gypsum particles broken up by the sonication process. Although the hydration results in Figure 1d were similar for both types of sonicated samples, image analysis of the 60 minutes of hydration samples showed that those samples without SWCNT had a significantly higher percentage of the surface area of the cement grains covered with C_3A hydration products compared to those where the SWCNT samples were present (averages of 35% and 15% respectively). A second difference is that the prismatic hydration products that appear to be typical of cements before the end of the induction period have different aspects ratios in the two types of samples. Those seen in the samples without SWCNT (the dashed arrows in Figure 3 indicate typical examples seen at all early hydration times) had aspects ratios greater than 1 and were similar to those seen previously for as-delivered OPCs at the same stage of hydration[22]. In contrast, however, the samples with SWCNT typically have C_3A hydration products with aspect rations of 0.5 or less (dashed arrows, Figure 4a) and had larger diameters. Despite these effects, no evidence was observed for the formation of the early C_3A hydration products around SWCNT. Figure 4a also shows SWCNT bundles on the surface of the cement grains, including location where the bundles were crossing each other.

Examination of the samples with SWCNT at 135 minutes of hydration shows that the nanotube bundles appeared to be coated with hydration products (Figure 4b). In addition, calcium hydroxide crystals (not shown) were also easily identified at this stage of hydration. In contrast, the OPC samples sonicated without SWCNT (Figure 3) showed only small amounts of C-S-H at the same time period, again following the behaviour seen previously for the as-delivered cements[22].

By 180 minutes of hydration some grains retained the appearance seen at 135 minutes (Figure 4b), although the thickness of the structures was on average larger than that seen at earlier

times, while 25% of the grains had a more complex structure of hydration products, overlaying a larger pore structure (Figure 4c). At 240 minutes of hydration, the percentage of grains with the more complex structure had reached 75% and the structure was more developed, with deeper pores (Figure 4d). The samples without SWCNT at the same times had structures (Figure 5 shows 240 minute results) more typical of the as-delivered OPC, although the development of the hydration products appears to have been more rapid than in the corresponding as-delivered material[22].

By 24 hours of hydration the C-S-H hydration products had developed a much denser structure. Investigation of fracture surfaces produced by cracking the hydrated material showed examples of fibre pullout on 22 of the 24 samples examined. Figure 6 shows an example of fiber pullout with high density of SWCNT present on the fracture surface.

Finally, the calcium hydroxide content of the samples produced with and without SWCNT is shown in Figure 7. Within the uncertainty of the measurements, both samples had the same amount of $Ca(OH)_2$ at the same heat of hydration. This result indicated that the SWCNT accelerated the formation of C_3S hydration products, but did not affect the balance between the formation of calcium hydroxide and that of the other hydration products.

Discussion

A comparison of the results for the sonicated OPC (Figures 3 and 5) to those published previously for as-delivered OPC[22] shows that, despite the differences in the heat flow from the two types of sample, the underlying hydration behaviour was very similar. The same process of C_3A hydration products forming immediately after hydration, initial formation of C-S-H on the surface of the cement grain and gradual growth of those hydration products until they taken the form commonly seen in the literature occurred in each case. The differences in the hydration curves (Figure 1) between the as-delivered and sonicated OPCs were not, therefore, produced by

fundamental changes in the C-S-H hydration process. Instead, the sonication appears to have enhanced the initial C_3A hydration reactions (Figure 1d) and increased the coverage of the grain surface with resulting hydration products (35% versus 20% of the observed surface for the as-delivered OPC[22]). The increased coverage of the surface was likely responsible for the reduction in magnitude of peak 2 in Figure 1, as past work has suggested that the C_3A hydration products form on C_3S surfaces as well as on C_3A surfaces[22], competing for nucleation sites with C-S-H. Figure 3 shows examples of C_3A hydration products formed on a C_3S surface (identification by energy dispersive X-ray dispersive analysis in the SEM). The C_3A hydration products may also have inhibited the dissolution of material below C_3A hydration product covered surfaces, resulting in the lower value of peak 3. In addition, the broadening of peak 4 (Figure 1a,d) may be explained as being due to the combination of the existence of a higher number of nucleation sites for further C_3A reactions as compared to the as-delivered OPC, which would accelerate the start of those reactions, and the likely location of the existing hydration products over regions of C_3A, slowing the peak 4 reactions once they have initiated.

The porosity observed before the induction period in the sonicated OPC (25% of the observed surface area) suggests that the sonication process also enhanced the dissolution of the C_3S in the samples. The porous surface area was too high to represent only areas of C_3A and the structure of the pores was similar to that observed previously during the dissolution of C_3S[22]. However, no C-S-H formation was observed before the end of the induction period and the calcium ion content was lower in the sonicated samples pore water than that of the as-delivered OPC paste. In combination with the conduction calorimetry measurements in Figure 1d, these results suggest that although the sonication process promoted the dissolution of the OPC surface before the end of the induction period, the resulting Ca^{2+} ions were consumed in the formation of the initial hydration products, rather than remaining in solution.The increased porosity in the

surface of the OPC grains may also be responsible for the increased concentration of Ca^{2+} ions in the pore water in the post-induction period as the dissolution process proceeds in part by creating pore growth during the main C_3S hydration reaction.[22] The increase presence of calcium ions during the initial stages of the main C_3S hydration reaction may in turn have resulted in the earlier timing of the maximum in the rate of change of the heat flow (peak 3, Figure 1e) for the two sonicated samples as compared to the as-delivered OPC, in the same manner that the addition of calcium chloride speeds the hydration process. However, further work is needed to fully understand the effect of sonication on OPC hydration.

The initial hydration reaction of the OPC sonicated with SWCNT produced as much or more heat than that in the sonicated OPC control sample, but produced less coverage of the exposed OPC surface by C_3A hydration products than was found for either the sonicated or the previously studied as-delivered OPCs. This result and the corresponding change in morphology of the C_3A hydration products (Figures 2 and 3) show that the SWCNT affected the C_3A hydration product formation. However, not only were no examples seen of those hydration products forming around SWCNT bundles, the reduction in aspect ratio of the C_3A hydration products in the presence of the SWCNT suggests that nanotubes acted to restrict the longitudinal C_3A hydration product growth, rather than promoting it. These factors suggest that the SWCNT on the surface of the OPC may have occupied many of the nucleation sites on the cementitious phases that would have otherwise been taken up by the C_3A hydration products. The presence of the nanotubes on the surface of the OPC grain may also have inhibited the longitudinal growth of the hydration products. As a consequence, the observed change in aspect ratio was driven by the formation of the same amount of C_3A hydration products as in the sonicated OPC sample in a significantly more restricted area. The greater degree of exposed C_3S surface area then permitted

an increased initial formation of C-S-H on the surface of the SWCNT, leading to the stronger peak 2 results seen in Figures 1a and 1d[22].

Once the main C_3S hydration reaction had started, the hydration products appear to have formed preferentially around the SWCNT. There was an acceleration of the reaction as compared to both the sonicated and as-delivered OPCs, as well as an increase in the rate of pore formation in the cement grain surfaces. A comparison between Figure 4 and Figures 3 and 5 as well as to the corresponding images in Makar and Chan[22] highlights the extent of the difference. Not only is there significantly more extensive pore formation at a given time when the SWCNT are present, but the location and structure of the C-S-H varies considerably between the two cases. The small, wisp-like structures (Figure 3) that are believed to be the initial stages of C-S-H formation on the surface of the OPC[22] were not identified in the samples with SWCNT. Instead, the network of rod-like structures on the surface of the OPC became thicker over time (Figure 4b). At later times, the surface of the grain appeared to have been mostly dissolved (Figures 4c and 4d) but an apparent network of C-S-H remained visible. This type of structure was not seen at any time in the case of the sonicated OPC control samples, which at 240 minutes of hydration (Figure 5) and a total heat of hydration of 12.5 J/g had the clustered appearance expected for as-delivered OPC hydration. In terms of total heat of hydration, the degree of reaction of the sonicated OPC sample at 240 minutes of hydration falls between that of the 180 minute (Figure 4c, 8.5 J/g heat of hydration) and the 240 minute (Figure 4d, 14.0 J/g heat of hydration) samples made with SWCNT. There was, however, no noticeable resemblance between the hydration product morphologies or degree of porosity between the two types of samples.

The pores seen in Figures 4c and 4d were present in all of the images examined and typically covered the entire surface visible at this degree of magnification. They therefore were

not simply due to the presence of a high degree of OPC grain porosity in the sample before the end of the induction period, as the samples sonicated without SWCNT showed a similar degree of porosity at that time, but their surface remained relatively intact at 240 minutes of hydration. While the early porosity undoubtedly played a role in the development of the overall porosity seen at 3 and 4 hours of hydration, a comparison with the results of the previous study suggests that the concentration of the C-S-H on and around the SWCNT in the samples studied here left more of the surface exposed to the aqueous environment around the OPC grains, allowing a higher degree of surface porosity to develop.It is clear from the data in Figures 1 and 4 that the presence of the SWCNT accelerates the hydration of the OPC. Hydration reactions can be accelerated both by chemical means such as the addition of Ca^{+} ions or through the addition of nucleating agents, which encourage the formation of the reaction products by providing sites for the reaction to occur. In OPC the initial nucleation sites are on the surface of the cement grains, while later sites are on the C-S-H itself. In both cases the process of nucleation may be facilitated by dangling chemical bonds. The situation on the surface of the cement grains is made more complex by the presence of dissolution sites as well as nucleation sites. The formation of distinct pores by dissolution processes as opposed to a general removal of material, strongly suggests the existence of preferred points of attack as dissolution occurs. Similarly, the localized growth of C-S-H on the surface of the cement grains indicates that there are specific sites on the grain surface that are more favourable to C-S-H formation than others. In as-delivered and sonicated OPC, large areas of grain surface remain clear of C-S-H formation until such time as the pores have grown to encompass them. In addition, the behaviour of peak 2 in Figures 1a and 1c and in previous work[22] suggests that the C-S-H and C_3A hydration products may nucleate on the same sites, as increasing C_3A hydration products inhibit C-S-H surface formation.

SWCNT are chemically inert and are not consumed in the hydration reaction itself. The observed acceleration of the hydration reaction was therefore likely due to nucleation effects, with the nanotubes having enhanced the rate of the hydration reactions by acting as a matrix for the formation of the C-S-H and/or calcium hydroxide produced in the hydration process. Other examples can be found in the literature where accelerated hydration has been attributed to nucleation effects[32]. The behaviour observed in the SEM images, where the C-S-H formed preferentially around the SWCNT bundles, supports the concept of the nanotubes as nucleating agents.

Nanotubes have been identified as nucleating agents for a variety of materials, including nanodiamonds[33] grown on SWCNT and titanium dioxide[34], silicon nitride[10], zirconium oxide[35], and calcium carbonate[36] grown on multiwalled carbon nanotubes. There is also a growing literature on effects of nanotubes on the nucleation and growth of hydroxyapatite cements[37-41]. In most of this work, the nanotubes were functionalized before use and the nucleation process was generally considered to be initiated by reaction with the functional groups. There were, however, examples where nucleation on the nanotubes by the ceramic appeared to take place without the aid of functional groups[32-34]. In these cases the occurrence of the nucleation was noted, but the actual nucleation process was not explained.

The research presented here differs from that involving the other materials, however, in that the SWCNT are located on the surface of the cement grains. None of the other materials are produced from a bulk precursor in contact with the nanotubes, although many of the apatite production methods involve aquaeous precursor ions that produce hydration products on the nanotube surface. A second significant difference from the various ceramic composites is that the hydration products appear to evenly coat the nanotube bundles, creating a gradually increasing layer of C-S-H around the SWCNTs, rather than single crystals growing out from their

sides. A exception is the work on titanium dioxide[34], where a sol-gel method was used to deposit alkoxides on the surface of MWCNTs, followed by heat treatment to remove the organic components of the deposited material. In that case an even ceramic coating along the length of the nanotubes was also obtained. A final difference between the work with other ceramics and that presented here is that the current method of purification of the SWCNTs[24] would be expected to produce a minimal amount of unintentional functionalization. Common methods relying on acid or base washes as part of the purification process may produce functional moities on the surface of the nanotubes. The solvent based method here would be expected to avoid such unintended functionalization, leaving lattice defects as the likely remaining source of dangling bonds on the nanotube surface.

The preferential nucleation of the C-S-H on the SWCNT bundles raises questions about the mechanism of nucleation. Past work has shown that C-S-H can be nucleated on calcium carbonate with high surface areas[32], but there appeared to be some degree of chemical reactivity with the hydrating cement. Here there does not appear to have been a route for significant chemical bonding to take place. Despite the apparent lack of functional groups on the SWCNTs to promote nucleation, the preference for nucleation on the bundles was particularly marked. An examination of the sonicated control samples produced without SWCNT shows numerous C-S-H clusters on the surface of the OPC grains such as seen in Figures 5, while true clusters were almost impossible to identify in the samples with the nanotubes. It is possible that the reduction in C-S-H clusters on the surface was due to the SWCNT bundles occupying the relevant nucleation sites, as appeared to be the case with the early C_3A hydration. However, if that were the only mechanism occurring, C_3S hydration would likely begin at the same time or be slightly delayed in the same way as the data in Figure 1d as compared to the sonicated OPC alone, rather than accelerated as shown in Figure 1a. It would therefore appear that the nucleation on the

SWCNT occured preferentially, rather than because a reduced number of sites were available for the standard nucleation processes.

Moreover, the structure of the C-S-H on the nanotube bundles suggests that nucleation was either taking place relatively evenly along the length of the bundles or taking place at a few sites with rapid, preferential growth along the bundles until they were completely covered by the C-S-H. Localized growth from a few nucleation sites would be expected to produce less even C-S-H coatings, resulting in an appearance similar to that of sugar crystals grown on a string. The latter structure has been seen for hydroxyapatite[38] and zirconium oxide[35] deposited on MWCNTs.

Instead, two other processes may be driving the nucleation. First, electrostatic force measurements on SWCNTs distributed on a SiO_2 coating on a silicon substrate showed that the metallic nanotubes behaved as would be expected from electrostatic principles[42]. Electrostatic theory suggests that the local presence of ions near the metallic SWCNT may produce image charges and attractive forces that could draw the ions towards the nanotube surface[43]. This effect would be expected to continue even if the nanotube became charged due to contact with the dissolved ions. In addition, molecular dynamic studies suggest that water molecules may be trapped by polarization effects on the surface of SWCNTs[44]. It is therefore possible that both dissolved ions in the solution and the water needed to complete the reaction are being held by electrostatic forces against the nanotube walls, allowing the initial nucleation reactions to take place. Second, studies of as-produced[45] and acid purified MWCNT[45,46] have shown that both have a strong ability to adsorb metallic ions, with results from chromium ion studies showing that the as-produced material has approximately half the adsorption ability as the acid treated material. SWCNT, with their higher surface areas per gram of material, should also have a higher adsorption capacity. Adsorption would also trap ions on the surface of the SWCNT bundles, again allowing the initial nucleation reactions to take place. In either case, the location

of the nanotubes on the surface of the cement grains may have enhanced the nucleation process by providing a continuing local source of ions and by trapping the ions in the narrow spaces between the bundles and the comparatively flat cement surface. Further work is needed to investigate these possible mechanisms. In particular, while TEM investigation of the C-S-H on the cement grain surfaces is difficult due to the location of the nanotubes, studies of synthetic C-S-H nucleation on SWCNTs would allow for TEM studies of both the bond between the nanotubes and the C-S-H and the nucleation process itself.

The nucleating effects of the SWCNT in combination with their effect on the formation of the initial C_3A hydration products also appears to be responsible for the increased heat produced during peaks 3 and 4 in Figure 1a as compared to the sonicated and as-delivered OPC samples. As noted earlier, in the case of the sonicated OPC without SWCNT, a much higher percentage of the OPC grain surface is covered with early C_3A hydration products, which appear to inhibit the dissolution of the unhydrated material in the grains, resulting in the reductions in the peaks produced by the sonicated OPC as compared to that produced by the as-delivered material. In the case of the samples sonicated with SWCNT, the surface area covered by the early C_3A hydration products is substantially reduced, improving access to the surface of the grains by the mix water. The nucleation of the C-S-H on the SWCNT continued that improved access, resulting in the increased dissolution of the grain surfaces that produced the porosity in Figures 4d and 4e, which in turn produced an accelerated hydration process and the increase heat flow associated with peak 3 seen in Figure 1a for this sample. Similarly, the enhanced peak 4 can be attributed to increased access to regions of C_3A on the surface of the grains, again accelerating the associated hydration reaction.

Finally, the nucleation of C-S-H by the SWCNT bundles also explains why the nanotubes appear to act as reinforcements in the matrix, rather than as crack formers. Without some form of

bonding between the matrix and the nanotubes, crack forming behaviour by the SWCNT would be expected to leave them exposed as bundles lying along the former original grain surfaces. Instead, the visible fiber pullout behaviour in the samples indicates that the matrix had failed across the SWCNT bundles, with an end of each bundle remaining bonded to the matrix as the previously attached material was pulled away (Figure 6). Development of the strength of the matrix has been seen to increase this effect to the point where the C-S-H was held together by the SWCNT, leading to crack bridging behaviour[20]. As the SWCNT were not functionalized, the presence of these classical reinforcing mechanisms suggest a high degree of interfacial bonding between the two materials. The porous nature of C-S-H means that contact between it and the SWCNT during the normal process of hydration would be unlikely to produced the needed level of interfacial contact. Direct nucleation on the bundles would, however, produce a dense C-S-H structure against the surfaces of the nanotubes that would be capable of producing the observed level of reinforcing behaviour.

Conclusions

Unfunctionalized SWCNT bundles distributed by sonication in isopropanol on OPC grains accelerated the hydration of the OPC as compared both to OPC control samples sonicated alone and to as-delivered OPC. The morphology and location of the C_3A hydration products was altered by the presence of the SWCNT, but no evidence was observed for the nucleation of the C_3A hydration products on the SWCNT bundles. C_3S hydration reactions were instead responsible for the observed change in hydration behaviour. Both the initial C_3S hydration peak at the end of the induction period and the bulk C_3S hydration peak were increased in magnitude. In addition, formation of calcium hydroxide during the hydration reaction was enhanced during the first 24 hours of hydration, with the increase in the calcium hydroxide directly reflecting the increased heat of hydration of the SWCNT composite as compared to the sonicated control.

SEM images showed the preferential formation of C-S-H on the surface of the nanotube bundles in the form of a gradually thickening coating. Similar structures were not seen in either type of control sample. The combination of accelerated hydration reactions, increased production of calcium hydroxide, and formation of hydration products around the nanotubes indicates that the SWCNT nucleated the hydration reactions, possibly through polarization or adsorption effects. The nucleation of the C-S-H on the SWCNT slowed the formation of a coating of C-S-H on the surface of the OPC grains, resulting in enhanced dissolution and nucleation and growth hydration activity as compared to both the as-delivered and sonicated OPC samples.

Images taken at 24 hours of hydration showed evidence of classical reinforcing behaviour, including fiber pullout and two pieces of hydration product held together by SWCNT bundles. The evidence for classical reinforcing behaviour and the formation of the C-S-H on the SWCNT bundles suggests that there is a significant degree of interfacial bonding between the C-S-H and the SWCNT. The results presented here therefore indicate strong potential for the development of high strength cement/SWCNT composites.

References

1. M.-F. Yu, O. Lourie, M. J. Dyer, K. Moloni, T. F. Kelly, and R. S. Ruoff, "Strength and Breaking Mechanism of Multiwalled Carbon Nanotubes Under Tensile Load", *Science*, **287**, 637-640, 2000.
2. J.-P. Salvetat, J.-M. Bonard, N. H. Thomson, A. J. Kulik, L. Forró, W. Benoit, and L. Zuppiroli, "Mechanical Properties of Carbon Nanotubes", *Appl. Phys. A*, **69**, 255-260, 1999.
3. D. A. Walters, L. M. Ericson, M. J. Casavant, J. Liu, D. T. Colbert, K. A. Smith, R. E. Smalley, "Elastic strain of freely suspended single-wall carbon nanotube ropes" App. Phys. Let., **74,** 3803-3805, 1999.

4. L. X. Zheng, M. J. O'Connell, S. K. Doorn, X. Z. Liao, Y. H. Zhao, E. A. Akhadov, M. A. Hoffbauer, B. J. Roop, Q. X. Jia, R. C. Dye, D. E. Peterson, S. M. Huang, J. Liu & Y. T. Zhu, "Ultralong single-wall carbon nanotubes", *Nat. Matr.*, **3,** 673-676, 2004.
5. J. N. Coleman, U. Khan, W. J. Blau, Y. K. Gun'ko., "Small but strong: A review of the mechanical properties of carbon nanotube–polymer composites", *Carbon*, **44**, 1624-1652, 2006.
6. T. Kuzumaki, O. Ujiie, H. Ichinose, K. Ito, "Mechanical Characteristics and Preparation of Carbon Nanotube Fiber-Reinforced Ti Composite", *J. Matr. Res.*, **13,** 416-418, 2000.
7. G.-D. Zhan, J.D. Kuntz, J. Wan and A. K. Mukherjee, "Single-wall carbon nanotubes as attractive toughening agents in alumina-based nanocomposites", *Nat. Mater.*, **2**, 38-42, 2002.
8. Z. Xia, L. Riester, W.A. Curtin, H. Li, B. W. Sheldon, J. Liang, B. Chang, J.M. Xu, "Direct observation of toughening mechanisms in carbon nanotube ceramic composites", *A. Mater.*, **52**, 931-944, 2004.
9. T. Wei, Z. Fan, G. Luo, F. Wei, "A new structure for multi-walled carbon nanotubes reinforced alumina nanocomposite with high strength and toughness", *Mat. Let.*, **62** 641-664, 2008.
10. Cs. Balázsi, F. Wéber, Zs. Kövér, Z. Shen, Z. Kónya, Zs. Kasztovszky, Z. Vértesy, L.P. Biró, I. Kiricsi, P. Arató, "Application of carbon nanotubes to silicon nitride matrix reinforcements", *Cur. Appl. Phys.*, **6**, 124-130, 2006.
11. H.F.W Taylor, ch. 5 and 6 in *Cement Chemistry* 2nd Ed., Thomas Telford, London (1997)
12. Campillo, J. S. Dolado, A. Porro, "High performance nanostructured materials for construction", Nanotechnology in Construction (Proceedings of the First International Symposium on Nanotechnology and Construction, 23rd-25th June, 2003, Paisley,

13. Y. S. De Ibarra, J. J. Gaitero I. Campillo, "Atomic force microscopy and nanoindentation of cement pastes with nanotube dispersions", *phys. stat. sol. (a)*, **203**, 1076-1081, 2006.

14. G. Y. Li, P. M. Wang, X. Zhao, "Mechanical behaviour and microstructure of cement composites incorporating surface-treated multi-walled carbon nanotubes", *Carbon*, **43** 1239 – 1245, 2005.

15. X. J. Xiang, T. L. Torwald, T. Staedler, R. H. F. Trettin, "Carbon nanotubes as a new reinforcement material for modern cement-based binders", *NICOM2* (Proceedings of the Second International Symposium on Nanotechnology and Construction, 13th-16th November 2005, Bilbao, Spain), 209-213, 2005.

16. Cwirzen, A., Habermehl-Cwirzen, K. and Penttala, V., Surface decoration of carbon nanotubes and mechanical properties of cement/carbon nanotube composites, *Ad. Cem. Res.*, **20**, 65-73, 2008.

17. G. Y. Li, P. M. Wang, X. Zhao, "Pressure-sensitive properties and microstructures of carbon nanotube reinforced cement composites", *Cem. Conc. Comp.*, **29**, 377-382, 2007.

18. S. Wansom, N. J. Kidner, L. Y. Woo, T. O. Mason, "A.C.-impedance response of multi-walled carbon nanotube/cement compositesm, *Cem. Conc. Comp.*, **28**, 509-519, 2006.

19. H.F.W Taylor, p. 133 in *Cement Chemistry* 2nd Ed., Thomas Telford, London (1997)

20. J. M. Makar, J. Margeson and J. Luh, "Carbon nanotube/cement composites – early results and potential applications", Construction Materials (Proceedings of ConMat '05 and Mindess Symposium, Vancouver, Canada, August 22-24, 2005, editors N. Banthia, T. Uomoto, A. Bentur and S.P. Shah), UBC Press, Vancouver, Canada, 32, 2005.

21. Beaudoin, J.J. and Feldman, R.F., "A study of mechanical properties of autoclaved calcium silicate systems, *Cem. Conc. Res.*, **5**, 103-118, 1975.

22. J.M. Makar and G.W. Chan, "End of the induction period in ordinary Portland cement as examined by high resolution scanning electron microscopy," *J. Amer. Ceram. Soc.,* **91**, 1292-1299, 2008.

23. C.T. Kingston, Z.J. Jakubek, S. Denommee and B. Simard, "Efficient laser synthesis of single-walled carbon nanotubes through laser heating of the condensing vaporization plume", *Carbon*, **42**, 1657-1663, 2004.

24. C.T. Kingston, C.M. Homenick, J. Guan, and B. Simard, "Nondestructive purification of single-walled carbon nanotubes using simple solvents", in preparation.

25. C. Gallé, "Effect of drying on cement-based materials pore structure as identified by mercury intrusion porosimetry: A comparative study between oven-, vacuum-, and freeze drying", *Cem. Concr. Res.*, **31,** 1467-1477, 2001.

26. A. Korpa and R. Trettin, "The influence of different drying methods on cement paste microstructures as reflected by gas adsorption: Comparison between freeze-drying (F-drying), D-Drying , P-drying and oven drying methods", *Cem. Concr. Res.*, **36,** 634-649, 2006.

27. J.M. Makar, G.W. Chan, and K.Y. Esseghaier, "An Additional Hydration Reaction at the End of the Cement Induction Period", *J. Mater. Sci.,* **42,** 1388-1392, 2007.

28. J.M. Makar and G.W. Chan, "Derivative Conduction Calorimetry", *Proceedings of the 12th International Congress on the Chemistry of Cement*; edited by J.J. Beaudoin, J.M. Makar and L. Raki; ST2: Characterization Techniques, Session W2-05: Thermal Analysis; paper: W2-05.3, published by the National Research Council of Canada; Montreal Canada; July 2007.

29. P.L. Pratt and A. Ghose, "Electron microscope studies of Portland cement microstructures during setting and hardening", *Phil. Trans. R. Soc. Lond. A*, **310,** 93-103, 1983.

30. P. Barret and D. Bertrandie, "Importance of the liquid to solid weight ratio in the powdered solid-liquid reactions: Example drawn from cement constitutent hydration", *Sol. Stat. Ion.,* **101-103**, 359-365, 1997.

31. H.F.W. Taylor, P. Barret, P.W. Brown, D.D. Double, G. Frohnsdorff, V. Johansen, D. Menetrier-Sorrentino, I. Odler, L.J. Parrott, J.M. Pommersheim, M. Regourd, and J.F. Young, "The hydration of tricalcium silicate", *Mater. et Cons.,* **17**, 457-468, 1984.

32. V.S. Ramachandran and Z. Chun-mei, "Dependence of fineness of calcium carbonate on the hydration behaviour of tricalcium silicate", *Dur. Build. Mater.*, **4**, 45-66, 1986.

33. M.L. Terranova, S. Orlanducci, A. Fiori, E. Tamburri, V. Sessa, M. Rossi, and A.S. Barnard, "Controlled evolution of carbon nanotubes coated by nanodiamond: the realization of a new class of hybrid nanomaterials", *Chem. Mater.*, **17**, 3214-3220, 2005.

34. A. Jitianu, T. Cacciaguerria, M.-H. Berger, R. Benoit, F. Beguin, S. Bonnamy, "New carbon multiwall nanotubes-TiO_2 nanocomposites obtained by the sol-gel method", *J. N. Crys. Sol.*, **345&346**, 596-600, 2004.

35. F. Lupo, R. Kamalakaran, C. Scheu, N. Grobert, and M. Rühle, "Microstructural investigations on zirconium oxide-carbon nanotube composites synthesized by hydrothermal crystallization", *Carbon*, **42**, 1995-1999, 2004.

36. D. Tasis, S. Pispas, C. Galiotis, and N. Bourpoulos, "Growth of calcium carbonate on non-covalently modified carbon nanotubes", *Matr. Lett.*, **61**, 5044-5046, 2007.

37. D. Tasis, D. Kastanis, C. Galiotis, and N. Bourpoulos, "Growth of calcium phosphate mineral on carbon nanotube buckypapers", *phys. stat. sol. (b),* **243**, 3230-3233, 2006.

38. T. Akasaka, F. Watari, Y. Sato, K. Tohji, "Apatite formation on carbon nanotubes", *Matr. Sci. Eng. C*, **26**, 675-678, 2006.

39. S. Aryal, S.R. Bhattarai, R. Bahadur K.C., M.S. Khil, D.-R. Lee, H. Y. Kim, "Carbon nanotubes assisted biomimetic synthesis of hydroxyapatite from simulated body fluid", *Matr. Sci. Eng. A,* **426**, 202-207, 2006.

40. B. Zhao, H. Hu, S.K. Mandal, R. C. Haddon, "A bone mimic based on the self-assembly of hydroxyapatite on chemically functionalized single-walled carbon nanotubes", *Chem. Mater.*, **17**, 3235-3241, 2005.

41. A.A. White, S. M. Best, and I. A. Kinloch, "Hydroxyapatite-carbon nanotube composites for biomedical applications: A review", *Int. J. Appl. Ceram. Technol.,* **4**, 1-13, 2007.

42. M. Paillet, P. Poncharal, A. Zahab, "Electrostatics of Individual Single-Walled Carbon Nanotubes Investigated by Electrostatic Force Microscopy", *Phys. Rev. Let.,* **94**, 186801, 2005.

43. J.D. Jackson, pg 54 in *Classical Electrodynamics*, 2nd Ed., John Wiley & Sons, New York, 1975.

44. F. Moulin, M. Devel, S. Picaud, "Molecular dynamics simulations of polarizable nanotubes interacting with water", *Phys. Rev. B*, **71**, 164501, 2005.

45. Z.-C. Di, Y.-H. Li, Z.-K. Luan, J. Liang, "Adsorption of chromium (VI) ions from water by carbon nanotubes", *Adsorp. Sci. & Tech.*, **22**, 467-474, 2004.

46. Y.-H. Li, J. Ding, Z. Luan, Z. Di, Y. Zhu, C. Xu, D. Wu, B. Wei, "Competitive adsorption of Pb^{2+}, Cu^{2+}, and Cd^{2+} ions from aqueous solutions by multiwalled carbon nanotubes", *Carbon*, **41**, 2787-2792, 2003.

Table

	Ca^{2+} Concentration (mmol/l, ±1)	
Time of Hydration	As-delivered OPC	Sonicated OPC
60 minutes	8	3
90 minutes	8	4
120 minutes	35	27
150 minutes	43	84
240 minutes	7	17

Table 1: Calcium ion content of as-delivered and sonicated OPC at early ages of hydration.

Figures

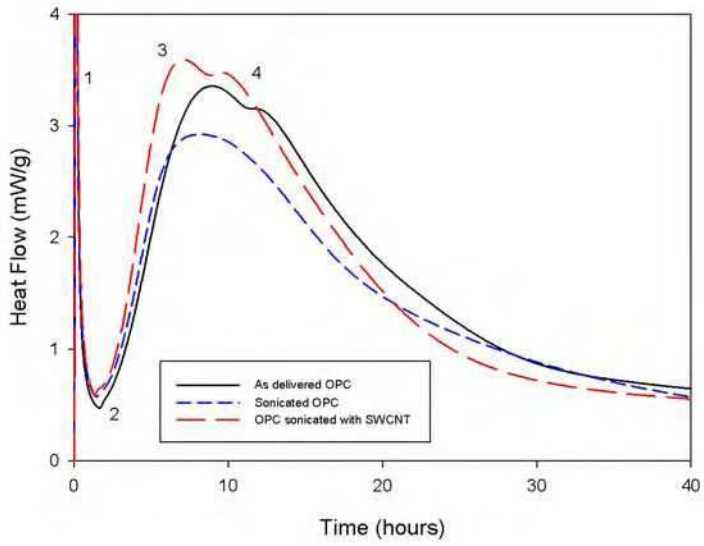

Figure 1a – Heat flow measured by isothermal conduction calorimetry. The numbers refer to various hydration reactions and are described in the text.

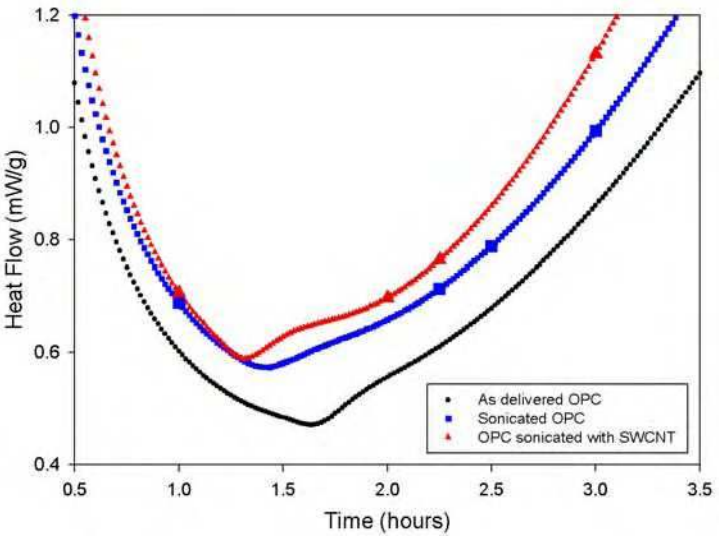

Figure 1b - Induction period heat flow, including peak 2., showing the measured data points (small symbols) and times chosen for SEM imaging (larger symbols). The times for the imaging of the as-delivered OPC are shown in elsewhere[22]. The uncertainty in the heat flow data is too small be shown.

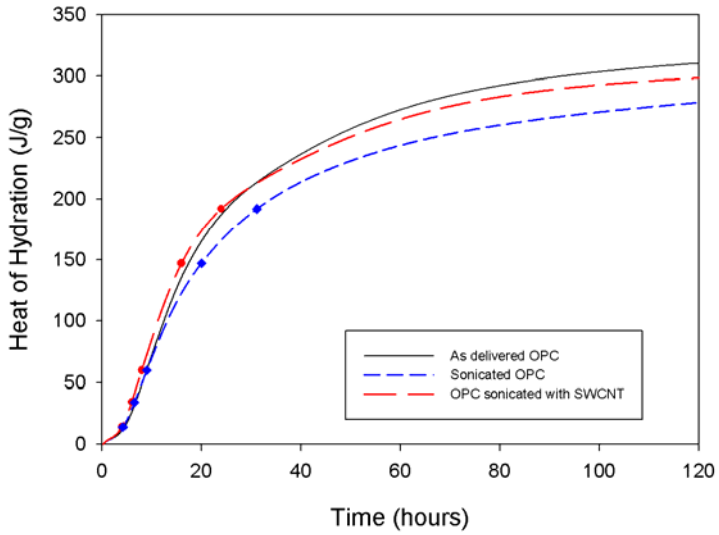

Figure 1c – Heat of hydration values calculated by integration of data in Figure 1a. The symbols indicate the times and heats of samples chosen for thermogravimetric analysis.

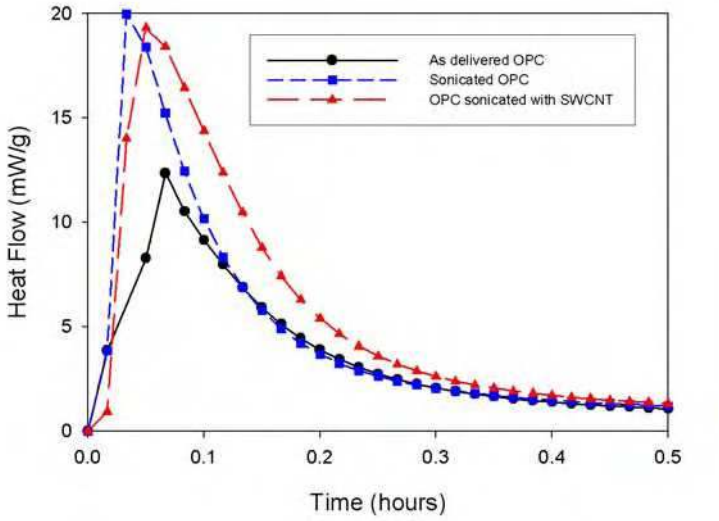

Figure 1d – Heat flow from C_3A reactions during the first half hour of hydration.

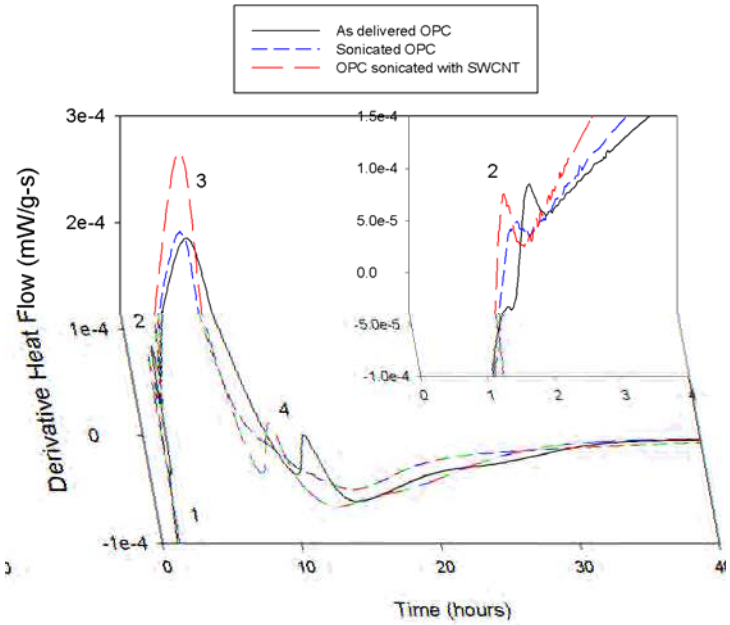

Figure 1e – Derivative values calculated from data in Figure 1a. The inset shows behaviour in the induction period. The numbers refer to the same events as in Figure 1a.

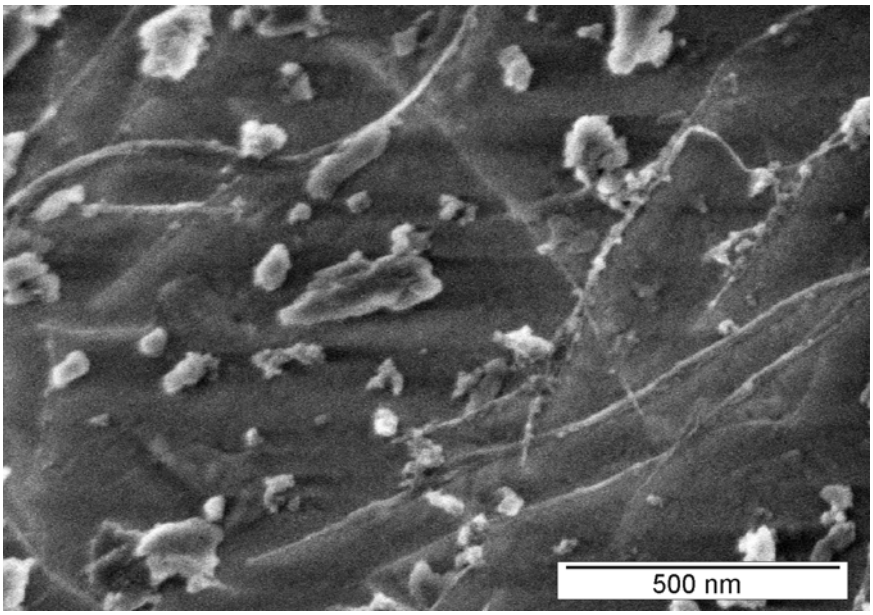

Figure 2 – SWCNT bundles (thin lines) on sonicated OPC grain surface (no hydration).

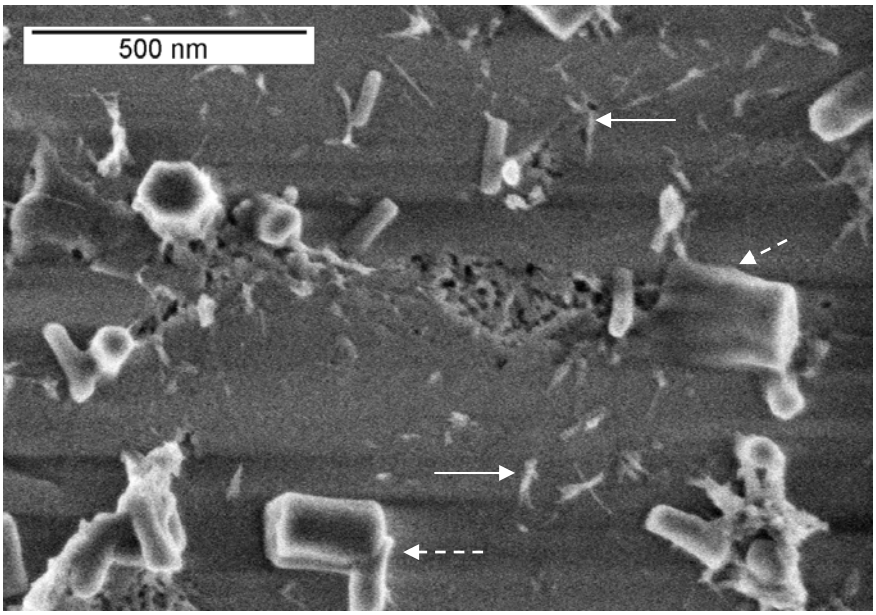

Figure 3 – OPC sonicated without nanotubes at 135 minutes of hydration. The solid white arrows points to likely examples of early C-S-H formation, while the dashed arrows indicate C_3A hydration products formed before the induction period.

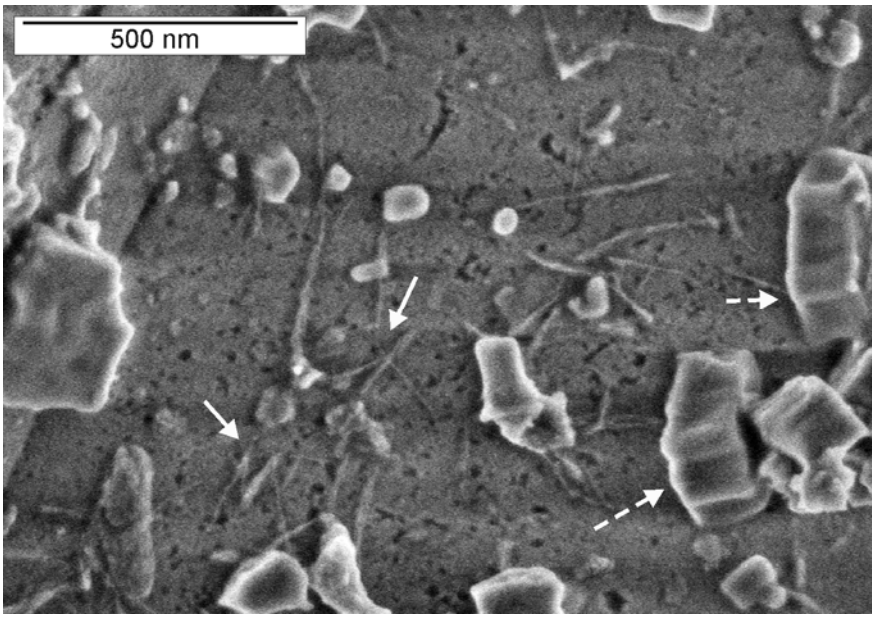

Figure 4a – Overlapping SWCNT structures (solid arrows) and early prismatic hydration structures (dashed arrows) at 60 minutes hydration.

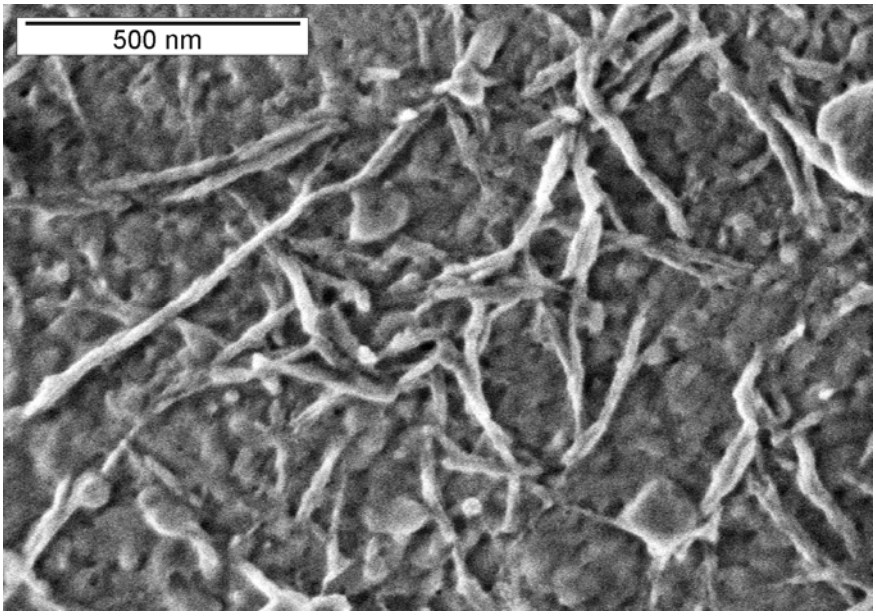

Figure 4b – Increased thickness of C-S-H on SWCNT bundles (135 minutes hydration).

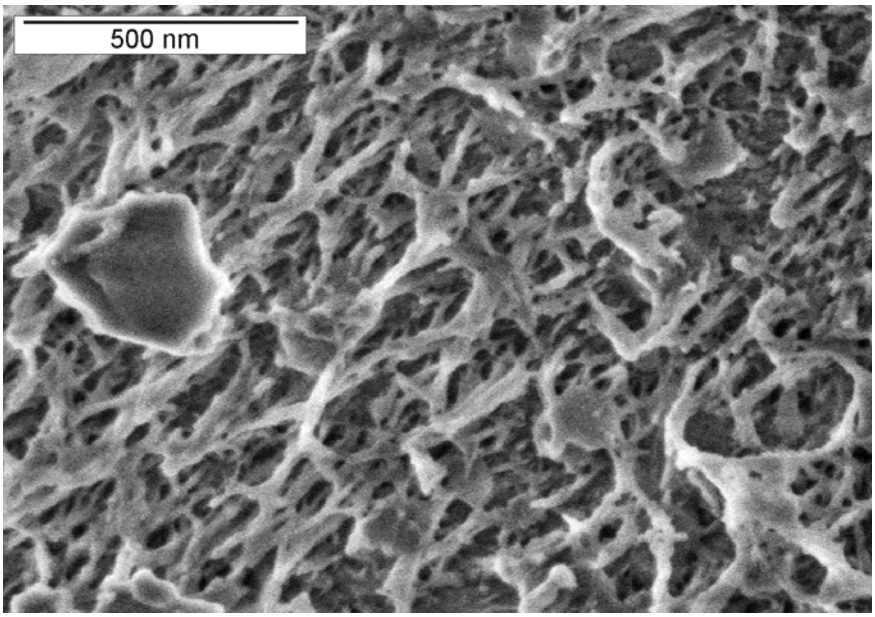

Figure 4c – Hydration product network on grain surface (180 minutes hydration).

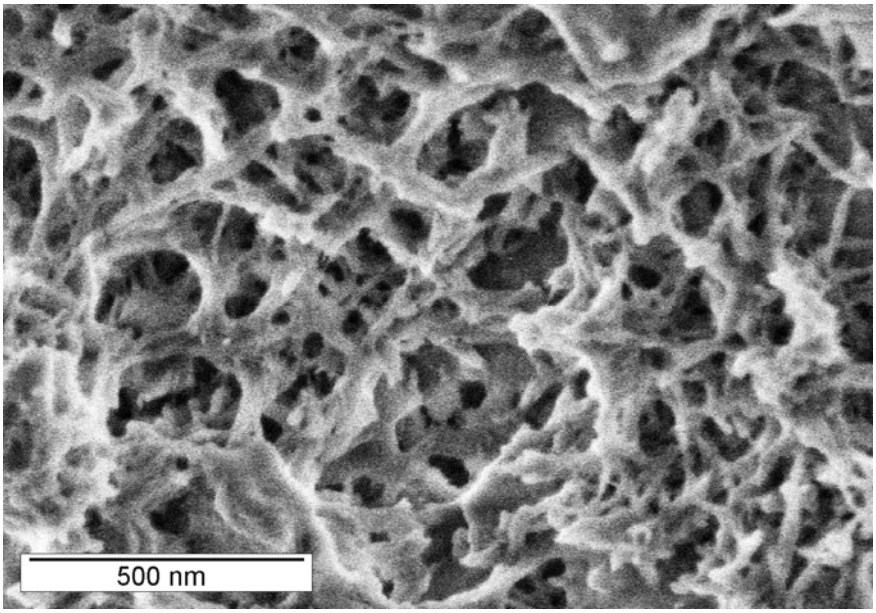

Figure 4d – Development of pore structure and hydration products (240 minutes hydration).

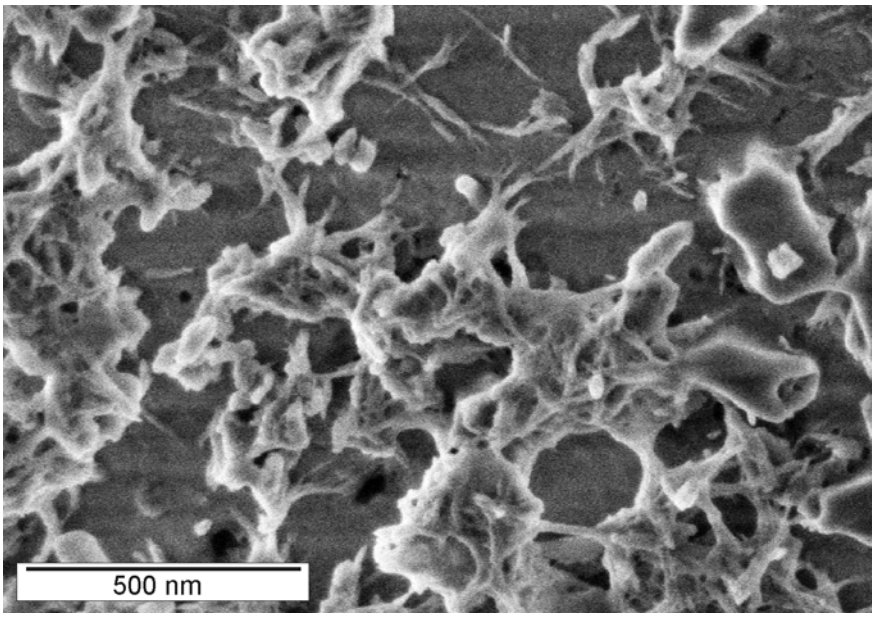

Figure 5 – OPC sonicated without nanotubes at 240 minutes of hydration, showing C-S-H clusters

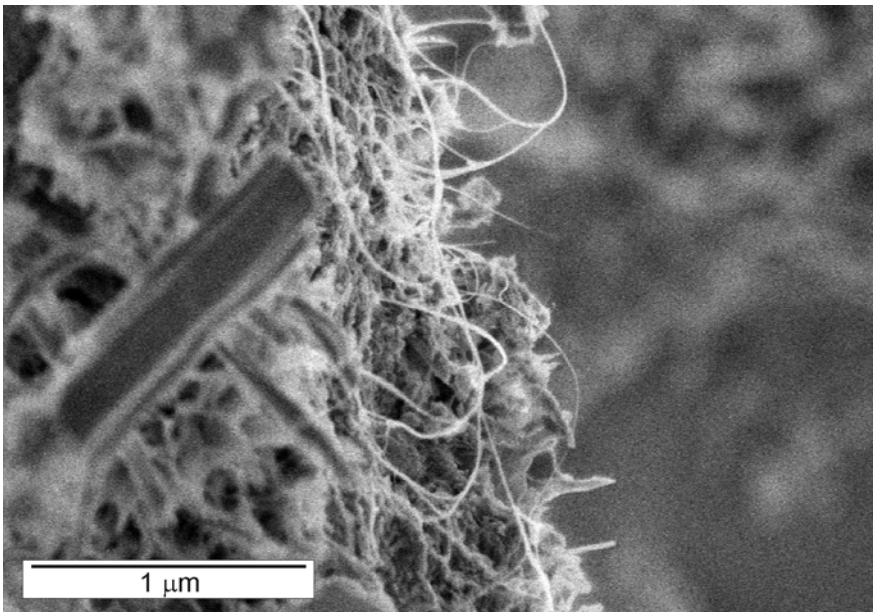

Figure 6 – Pulled out SWCNT bundles producing by cracking of composite sample at 24 hours of hydration.

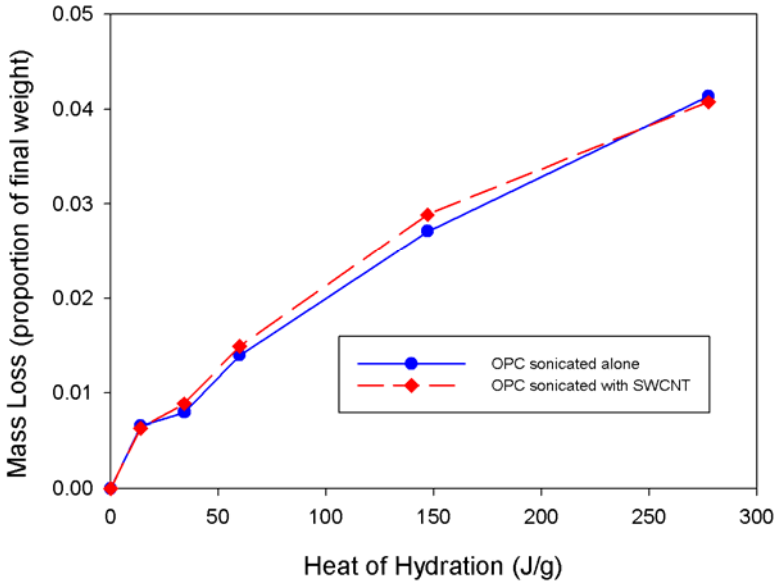

Figure 7 - Loss of mass due to calcium hydroxide decomposition. Sample times were chosen to have equivalent degrees of hydration, rather than the same time of hydration. The uncertainty in the measurement is ±0.001.